

Electronic Supplementary Information

Ionogel-Based Sodium Ion Micro-Batteries with a 3D Na-Ion Diffusion Mechanism Enable Ultrahigh Rate Capability

Shuanghao Zheng,^{abc} Huijuan Huang,^d Yanfeng Dong,^a Sen Wang,^{ac} Feng Zhou,^a

Jieqiong Qin,^{ac} Chenglin Sun,^a Yan Yu,^{*de} Zhong-Shuai Wu^{*a} and Xinhe Bao^{ab}

^aDalian National Laboratory for Clean Energy, Dalian Institute of Chemical Physics, Chinese Academy of Sciences, 457 Zhongshan Road, Dalian 116023, China. E-mail: wuzs@dicp.ac.cn

^bState Key Laboratory of Catalysis, Dalian Institute of Chemical Physics, Chinese Academy of Sciences, 457 Zhongshan Road, Dalian 116023, China

^cUniversity of Chinese Academy of Sciences, 19 A Yuquan Rd, Shijingshan District, Beijing, 100049, China

^dHefei National Laboratory for Physical Sciences at the Microscale, Department of Materials Science and Engineering, CAS Key Laboratory of Materials for Energy Conversion, University of Science and Technology of China, Hefei, Anhui, 230026, China. Email: yanyumse@ustc.edu.cn

^eState Key Laboratory of Fire Science, University of Science and Technology of China, Hefei, Anhui, 230026, China.

Methods

Materials Preparation. Urchin-like NTO was prepared from simultaneous alkalization and oxidation of Ti_3C_2 via hydrothermal treatment.¹ Briefly, Ti_3C_2 was obtained from the selective corrosion of Ti_3AlC_2 (Forsman, 98%, 200 mesh) etched by HF (Kermel, 40%, AR) at room temperature for 24 h. To achieve NTO, Ti_3C_2 (100 mg), NaOH (1 M, 30 mL, Kermel) and H_2O_2 (0.68 mL, Kermel, 30 wt%) were uniformly mixed. Then the resultant mixture was hydrothermally processed in Teflon-lined stainless-steel autoclave (50 mL) at 140 °C for 12 h. After washing and drying the white particles, NTO was achieved.

Flower-like carbon-coated NVP was synthesized by high temperature annealing.² Typically, 0.72 g V_2O_5 (Aladdin, 99%) and 1.52 g oxalic acid (Sinopharm, AR) were dispersed into deionized water at 70 °C. Subsequently, 1.84 g sodium dihydrogen phosphate (Sinopharm, AR) and 0.4 g glucose (Sinopharm, 99.5%) was added into the above dispersion, followed by the addition of 10 mL n-propanol (Sinopharm, 99.5%). After the obtained solution was dried, the mixture was heated at 800 °C for 6 h in 5% hydrogen atmosphere and NVP was obtained.

EG was prepared from the electrochemical exfoliation of graphite foil (0.13 mm, carbon content: 99.8%, Alfa Aesar) in aqueous 10 M KOH (Kermel, AR) solution, according to the previous work.³ Typically, graphite foil as anode (working electrode), using Pt foil as cathode (counter electrode), was exfoliated under a voltage of 10 V for 30 min. After that, the resultant product was collected and washed with deionized water. Finally, the exfoliated graphite was dispersed in alcohol (Kermel, AR) to form

EG solution under strong sonication with a power of 200 W for 30 min.

Ionogel Electrolyte. PVDF-HFP (0.1 g, Sigma-Aldrich, Mw of ~400,000 and Mn of ~130000) was dissolved into 2 g acetone (Sinopharm, AR) to form transparent dispersion. Then, 0.1g NaBF₄ (Sigma-Aldrich, 98%) dissolved into 1.6 g EMIMBF₄ (Lanzhou greenchem ILs, 99%) was dropwise added into the above solution. After continuously stirred for 2 h, NaBF₄-IE (NaBF₄-EMIMBF₄-PVDF-HFP ionogel electrolyte) was achieved. Similarly, NaTFSI-IE (NaTFSI-EMIMTFSI-PVDF-HFP ionogel electrolyte) was also obtained via the same approach, except using NaTFSI (0.27 g, WengJiang Reagent, 98%) and EMIMTFSI (1.7 g Lanzhou greenchem ILs, 99%), rather than NaBF₄ and EMIMBF₄.

Fabrication of NTO//NVP-NIMBs. Before the preparation of NIMBs, EG solution, NTO/EG dispersion and NVP/EG dispersion were prepared by strong sonication with a power of 200 W for 30 min. For the microelectrode fabrication, nylon membrane (AgelaTechnologies, 50mm, 0.22 μm) was firstly placed onto the sand core funnel, followed by the placement of the customized stainless steel interdigital mask (the length of 1.4 cm, width of 1 mm and interspace of 500 μm) with four fingers on each side and the height of 1cm. After the vacuum was opened, EG conductive layer was deposited on the nylon membrane via the filtration of 3 mL EG alcohol dispersion (0.1 mg/mL) from both sides of the customized mask. Then, NTO and NVP dispersion (0.5 mg/mL) with 10 wt% EG were deposited via each side of the same mask to form anode and cathode fingers, respectively. Then vacuum was closed and the interdigital microelectrodes on the nylon membrane were obtained. Subsequently,

the liquid precursor of the ionogel electrolyte (200 μL), e.g., $\text{NaBF}_4\text{-IE}$, was precisely coated on the area of the interdigital microelectrodes by a micro syringe with a diameter of 200 μm , and solidified at 80 $^\circ\text{C}$ for 12 h. Finally, the quasi-solid-state planar NIMBs, e.g., $\text{NTO}|\text{NaBF}_4\text{-IE}|\text{NVP}$, were achieved after the package with Kapton tape. To highlight the 3D multi-directional Na^+ ion diffusion mechanism, $\text{NTO}|\text{NaBF}_4\text{-IE}|\text{NVP}$ with extra thin EG cover on the top surface of negative ($\text{NTO}|\text{NaBF}_4\text{-IE}|\text{NVP-CN}$) or positive ($\text{NTO}|\text{NaBF}_4\text{-IE}|\text{NVP-CP}$) microelectrode side were designed using the dilute 3 mL EG dispersion (0.02 mg/mL) through the same filtration.

Materials Characterizations. The microstructure of NTO, NVP, EG, ionogel electrolyte and interdigital microelectrodes was characterized by XRD (X'pert Pro), SEM (JSM-7800F), TEM (JEM-2100), thermogravimetry (TG) measurement (STA 449 F3). The electronic conductivity of microelectrode films (NTO anode or NVP cathode) were measured by a four-point probe equipment (RTS-9). The ionic conductivity and transfer number of ionogel electrolyte in coin cell were calculated from the EIS results. *In-situ* Raman spectroscopy was performed on LabRAM HR 800 Raman spectrometer with 532 nm laser excitation.

Electrochemical Measurement. For the electrochemical performance test of NIMBs, the conductive Cu adhesive tape (SPI SUPPLIES) was used to connect microelectrode fingers with the external circuit, which was linked to the electrochemical workstation (CHI760E) for measurement. GCD measurements from 1 to 100 C and cycling stability at 20 and 60 C were tested by LAND CT2001A battery tester. The CV curves

from 1 to 10 mV/s and EIS spectra from 100 kHz to 0.01 Hz were performed on a CHI760E electrochemical workstation. The whole measurement of microdevices was carried out in a glovebox with an inert atmosphere. To high-temperature test, NTO//NVP-NIMBs-100 were maintained at 100 °C for 1 h until equilibration.

Calculation

The areal energy density and power density of NIMBs were calculated based on the footprint area (electrode fingers and interspace gaps, A_{area} (cm²)). The volumetric energy density and power density were evaluated based on the whole volume of electrodes, interspaces and ionogel electrolyte, V_{device} (cm³). The thickness of ionogel electrolyte was about 1.5 μm (Fig. S25).

The volumetric and areal capacities of NIMBs are evaluated according to GCD curves from the following equations (1) and (2):

$$C_{volume} = \frac{It}{V_{device}} \quad (1)$$

$$C_{areal} = \frac{It}{A_{device}} \quad (2)$$

Where C_{volume} (mAh/cm³) and C_{areal} (μAh/cm²) are the volumetric and areal capacity, respectively, I (mA) is the discharge current, t (h) is the discharge time.

The areal energy density and areal power density of NIMBs are calculated via the formula (3) and (4):

$$E_{areal} = \frac{I \int U dt}{A_{area}} \quad (3)$$

$$P_{areal} = \frac{E_{areal}}{t} \times 3600 \quad (4)$$

Where U (V) is voltage, E_{areal} (μWh/cm²) is areal energy density, and P_{areal} (μW/cm²) is areal power density.

The volumetric energy density and power density of NIMBs are calculated via the formula (5) and (6):

$$E_{volumetric} = \frac{I \int U dt}{V_{device}} \quad (5)$$

$$P_{volumetric} = \frac{E_{volumetric}}{t} \times 3600 \quad (6)$$

Where U (V) is voltage, $E_{volumetric}$ (mWh/cm³) is volumetric energy density, and $P_{volumetric}$ (mW/cm³) is volumetric power density.

The ionic conductivity of ionogel electrolyte was examined via the below equation (7):

$$\sigma = \frac{L}{R * S} \quad (7)$$

where σ (S/cm) is ionic conductivity. L (cm) and S (cm²) are the length and geometric area of ionogel electrolyte film, respectively. R (Ω) is ESR from EIS. EIS was tested from a cell architecture of stainless steel/NaBF₄-IE or NaTFSI-IE/stainless steel.

The Na⁺ ion transfer number (T_{Na^+}) is calculated from the results of EIS and $I-t$ curves according to the following equation (8):

$$T_{Na^+} = \frac{I^s(\Delta V - I^o R^o)}{I^o(\Delta V - I^s R^s)} \quad (8)$$

Where I^o and I^s are initial and stable current (A), respectively. ΔV is the voltage difference (V). R^o and R^s are the initial and steady-state charge transfer resistance (Ω), respectively.

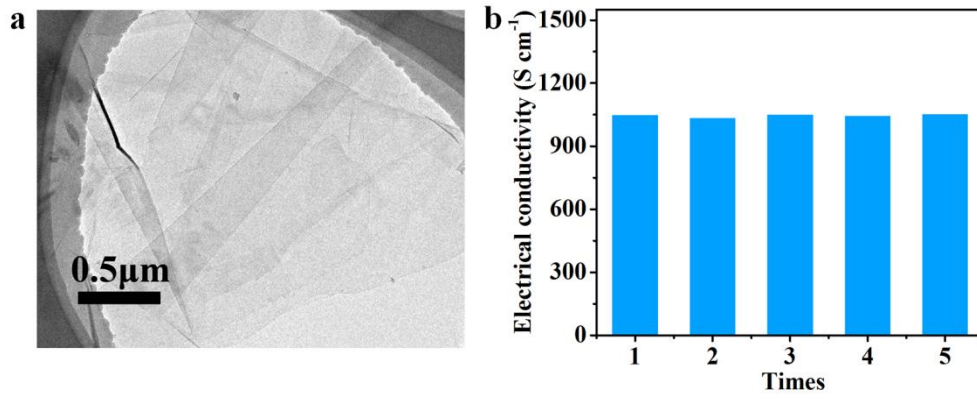


Figure S1. (a) TEM image of EG nanosheets with ultrathin and transparent structure. (b) Electrical conductivity of EG thin layer with a thickness of ~1.2 μm.

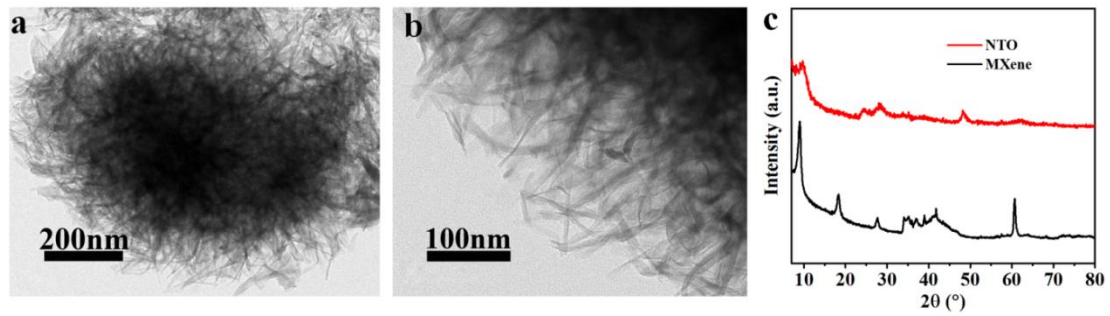


Figure S2. Morphology and structure of NTO. (a,b) TEM image of NTO. (c) XRD patterns of NTO and Ti₃C₂ MXene.

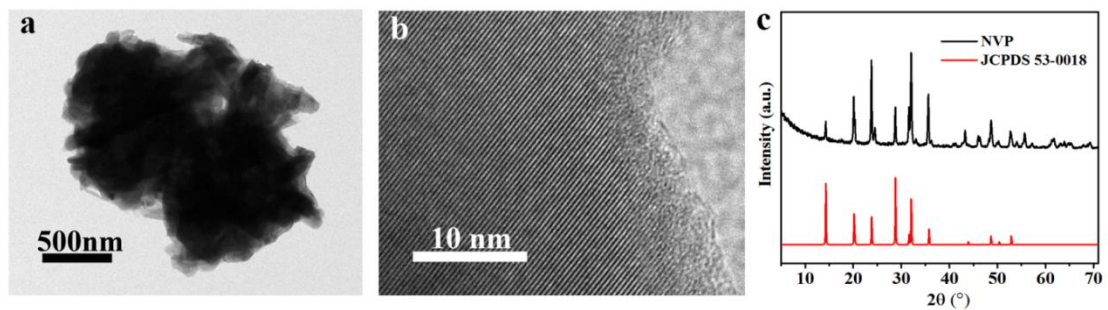


Figure S3. Morphology and structure of NVP. (a,b) TEM image with low (a) and high (b) magnification. (c) XRD patterns.

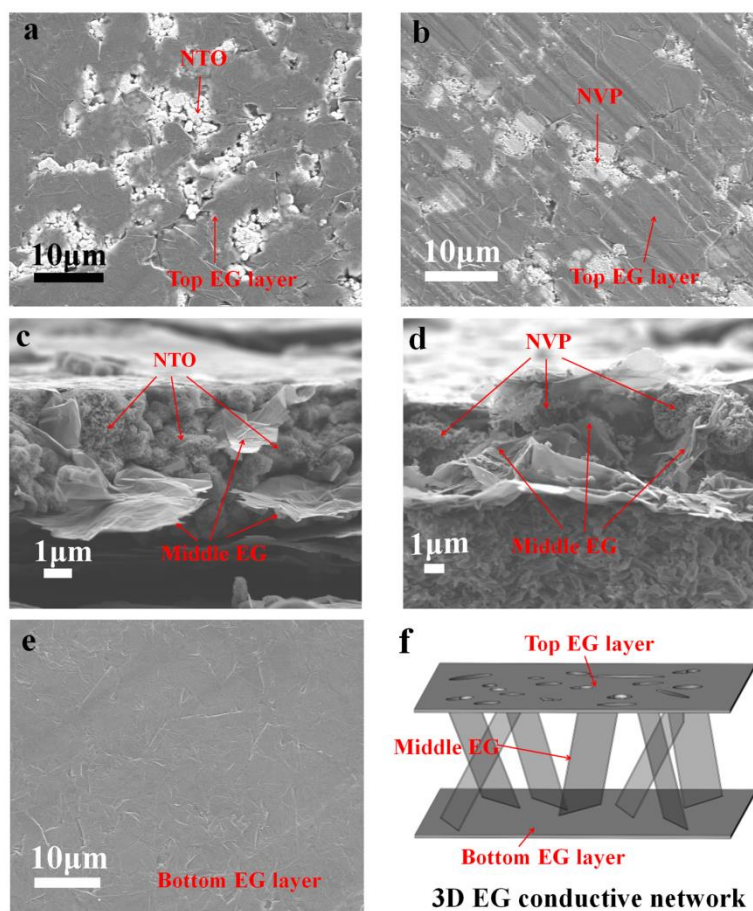


Figure S4. The morphology and structure of EG nanosheets in NTO anode and NVP cathode films. (a,b) Top-view SEM images of (a) NTO anode and (b) NVP cathode. (c,d) Cross-section SEM images of (c) NTO anode and (d) NVP cathode. (e) Top-view SEM image of the bottom EG current collector. (f) Schematic diagram of 3D highly conducting connected EG network. It is observed that the bottom, middle and top EG layers working together formed 3D highly conducting connected network, endowing NTO anode and NVP cathode films with high electrical conductivity of ~ 160 S/cm and ~ 180 S/cm, respectively.

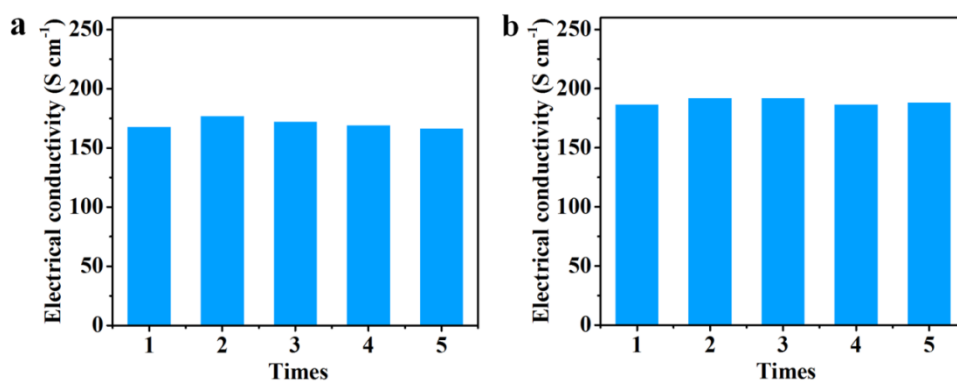


Figure S5. Electrical conductivity of NTO anode (a) and NVP cathode (b) films.

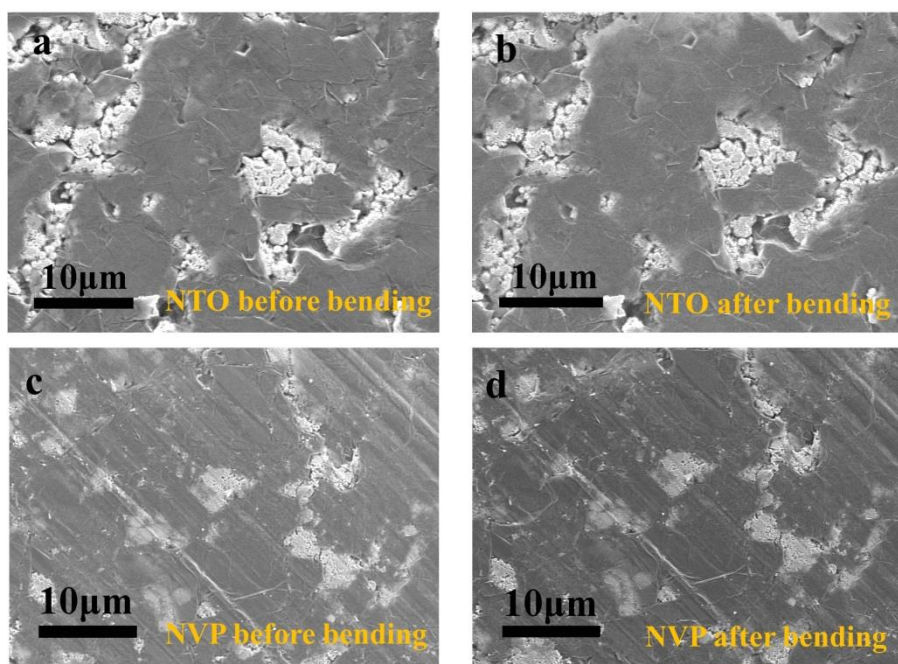


Figure S6. Top-view SEM images of NTO anode and NVP cathode microelectrode films (a,b) before and (c,d) after bending to be a circle (>180°). Both NTO anode and NVP cathode microelectrode films with EG layers displayed the highly intact and flat structure without any fracture, after they were highly bent to be a circle (> 180°), indicative of excellent structural integrity.

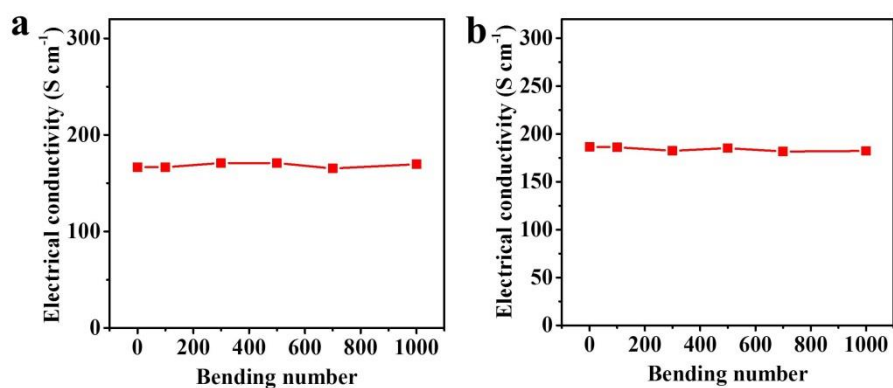


Figure S7. Electrical conductivities of (a) NTO anode and (b) NVP cathode films as a function of bending number. The electrical conductivities of anode ($\sim 160 \text{ S/cm}$) and cathode ($\sim 180 \text{ S/cm}$) films were kept unchanged before and after bending 1000 times, suggestive of highly conducting and stable microelectrodes.

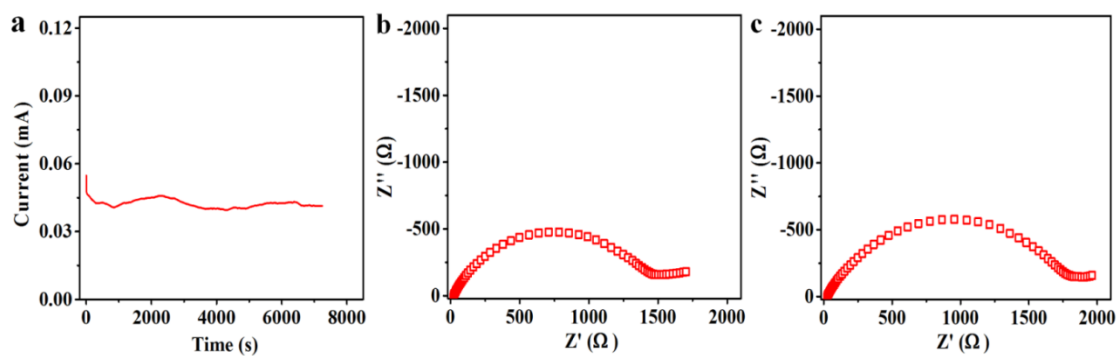


Figure S8. (a) The curve of current vs time during polarization of NaBF₄-IE. (b,c) Nyquist plots before (b) and after (c) polarization.

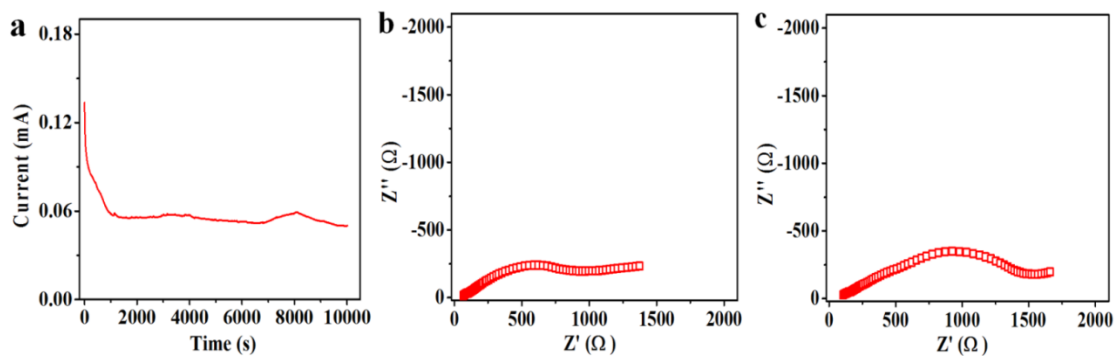


Figure S9. (a) The curve of current vs time during polarization of NaTFSI-IE. (b,c) Nyquist plots before (b) and after (c) polarization.

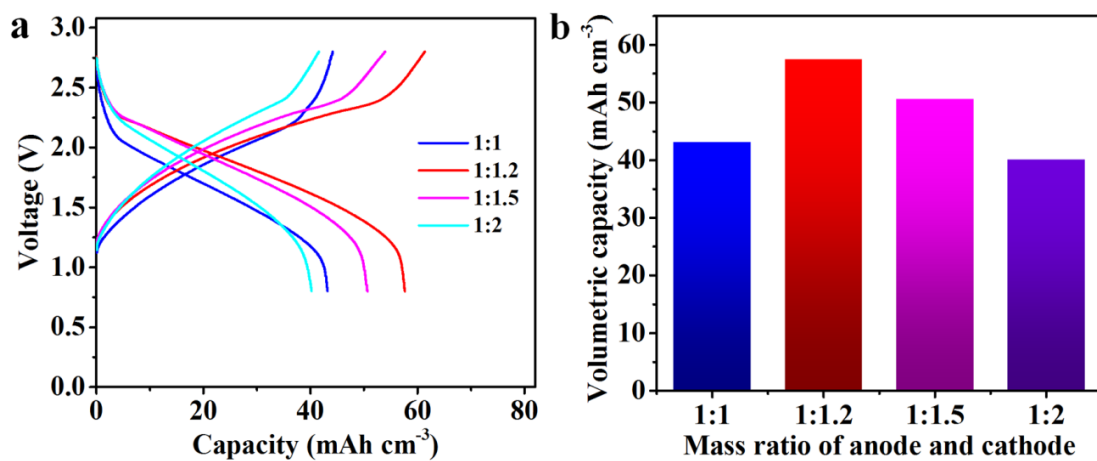


Figure S10. (a) GCD profiles and (b) volumetric capacity of NTO|NaBF₄-IE|NVP with different mass ratio of anode and cathode obtained at 1 C. These values were calculated based on the electrode volume.

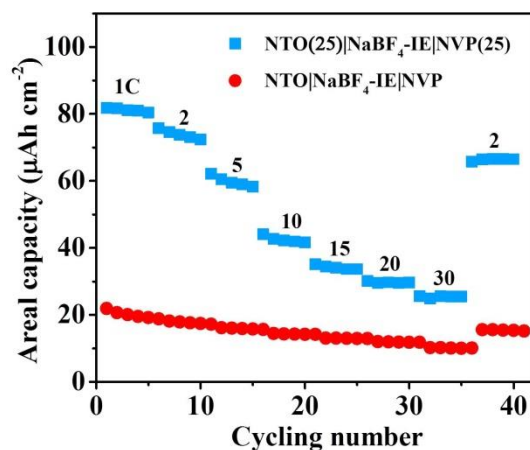


Figure S11. Areal capacity of NTO|NaBF₄-IE|NVP and NTO(25)|NaBF₄-IE|NVP(25) with different electrode thickness obtained at different rates.

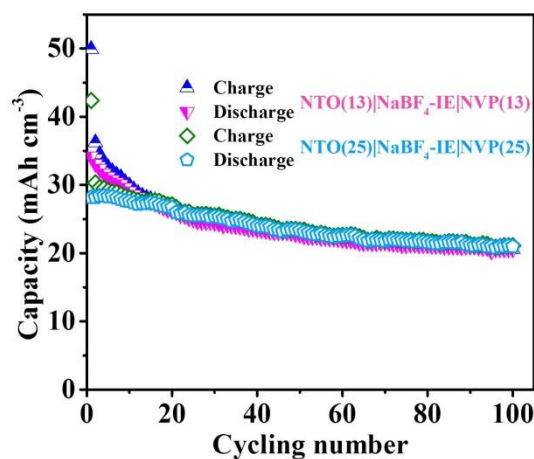


Figure S12. Cycling stability of NTO|NaBF₄-IE|NVP with different electrode thickness of 13 and 25 μm , obtained at a low rate of 1 C. It can be seen that NIMBs with the 13 μm -thick electrodes (denoted as NTO(13)|NaBF₄-IE|NVP(13)) presented high capacity retention of 60%. When the electrode thickness increased to 25 μm . NTO(25)|NaBF₄-IE|NVP(25) showed dramatically enhanced cyclability with higher capacity retention of 75%. The improved cyclability was likely attributed to the developed electron-ion conducting networks with assistance of high-conducting graphene in the thick electrode, which could accommodate the volume change of NTO and NVP and maintain the intact electrode structure during charge and discharge process.

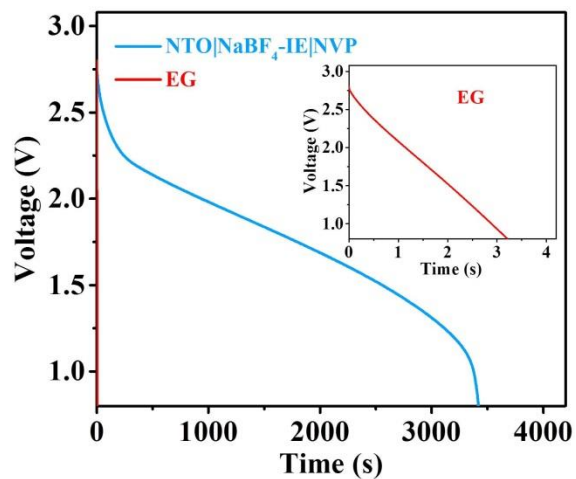


Figure S13. Discharged profiles of NTO|NaBF₄-IE|NVP and EG current collectors obtained at 0.03 mA cm⁻². Inset is the discharged profile of EG current collectors.

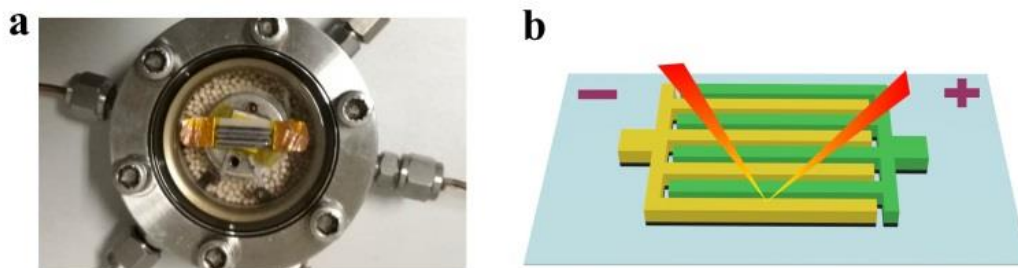


Figure S14. (a) Optical image of NIMBs of NTO|NaBF₄-IE|NVP for in-situ Raman experiment. (b) Schematic diagram of *in-situ* Raman spectroscopy.

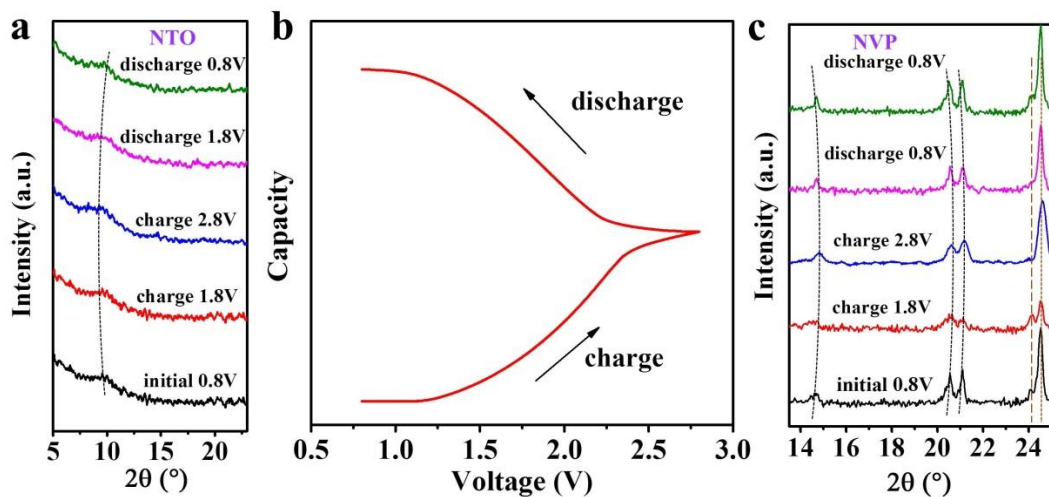


Figure S15. (a) *Ex-situ* XRD patterns of NTO anode measured at different voltages. (b) GCD profile measured at 1 C. (c) *Ex-situ* XRD patterns of NVP cathode obtained at different voltages.

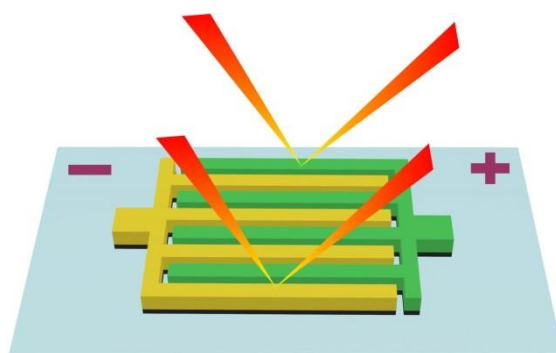


Figure S16. Schematic of planar microscale energy storage device as an ideal model for the *in-situ* characterization of both anode and cathode in a full cell simultaneously.

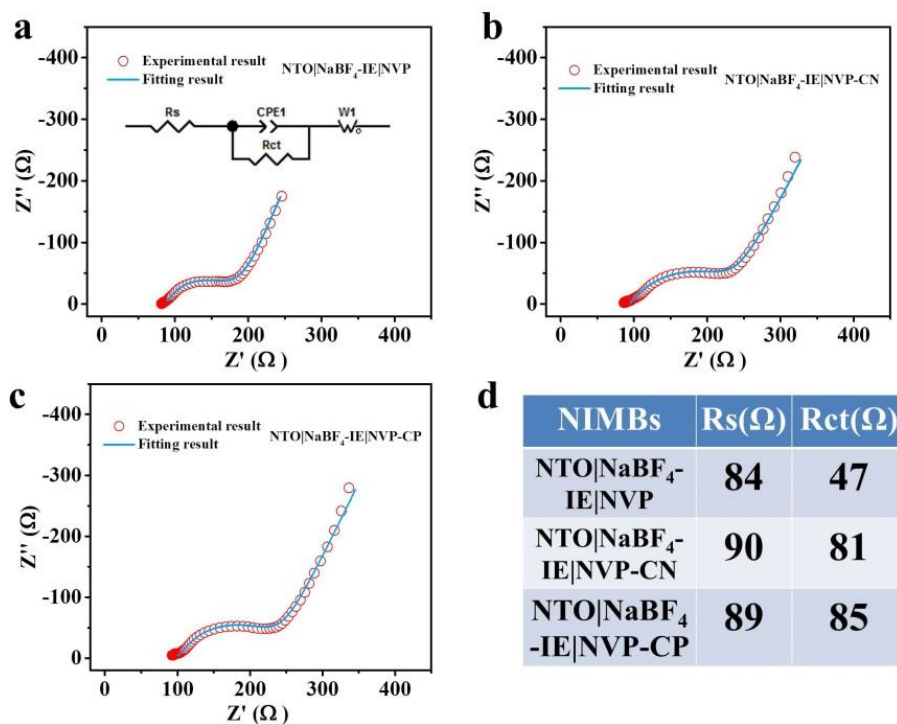


Figure S17. (a-c) EIS spectra and fitting results of NTO|NaBF₄-IE|NVP without EG cover (a), with EG cover on anode (b) and with EG cover on cathode (c). Inset in (a) is the equivalent circuit. (d) Comparison from the fitting results of EIS spectra.

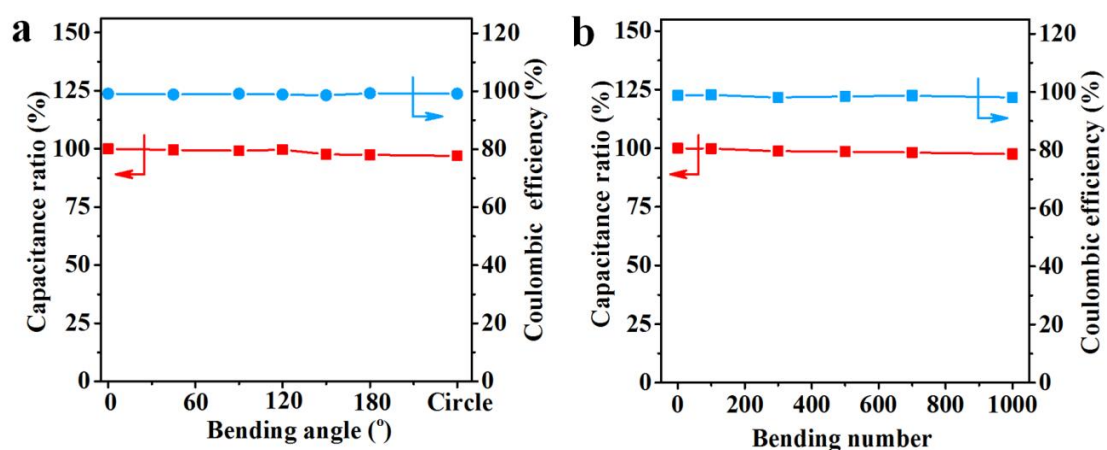


Figure S18. (a) Capacitance ratio vs bending angle from flat to circling state, and (b) capacitance ratio vs bending number of NTO|NaBF₄-IE|NVP.

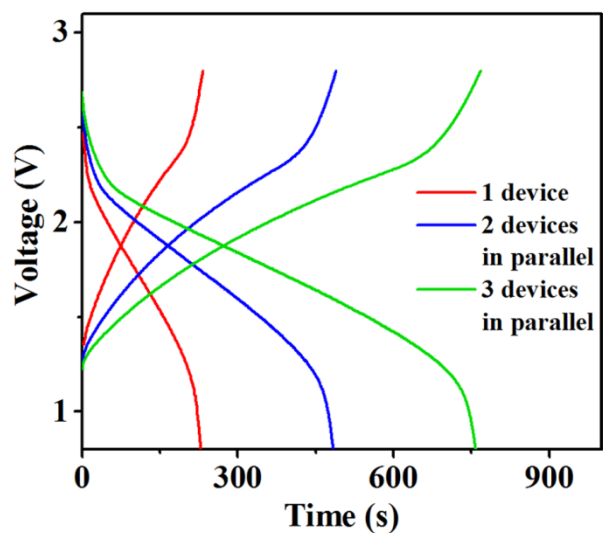


Figure S19. GCD profiles of parallel NTO|NaBF₄-IE|NVP with one, two and three cells.

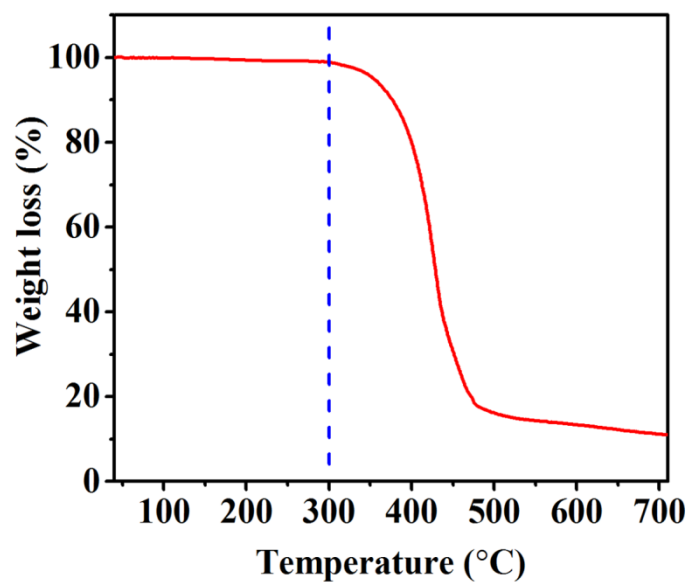


Figure S20. TG curve of NaBF₄-based ionogel electrolyte.

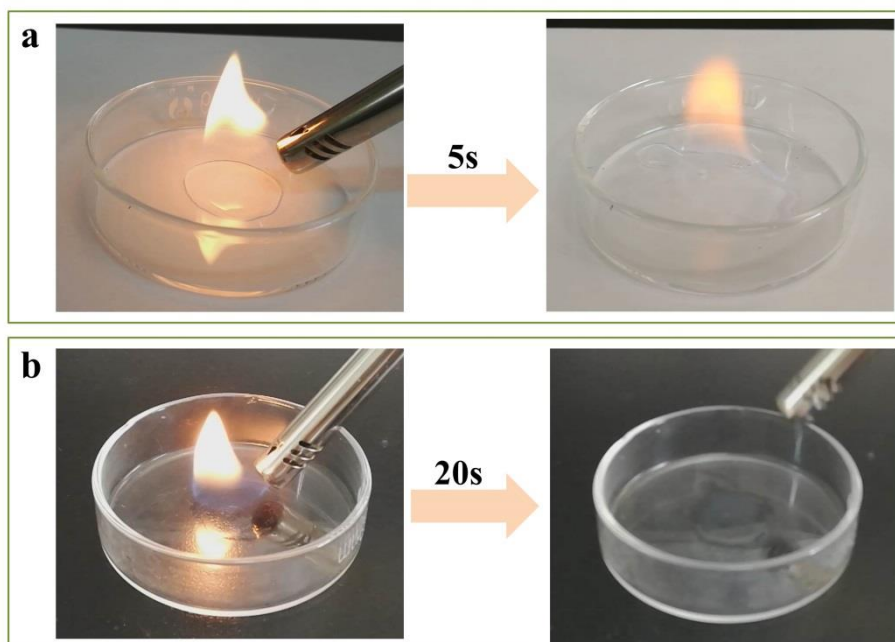


Figure S21. Flammable test of (a) commercial sodium ion gel electrolyte of NaPF₆ in diglyme mixed with PVDF-HFP, and (b) NaBF₄ based ionogel electrolyte.

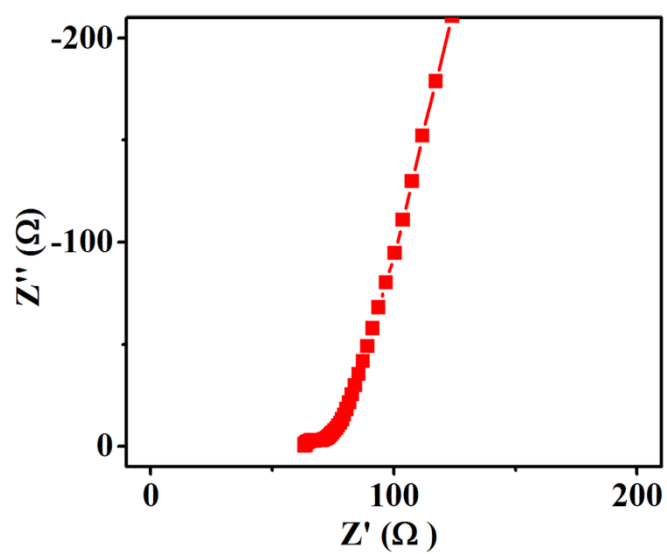


Figure S22. Nyquist plot of NTO|NaBF₄-IE|NVP-100.

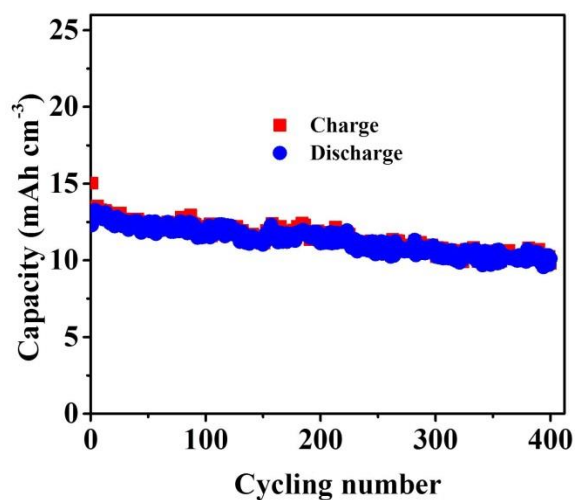


Figure S23. Cycling stability of NTO|NaBF₄-IE|NVP at 100 °C measured at current density of 60 C.

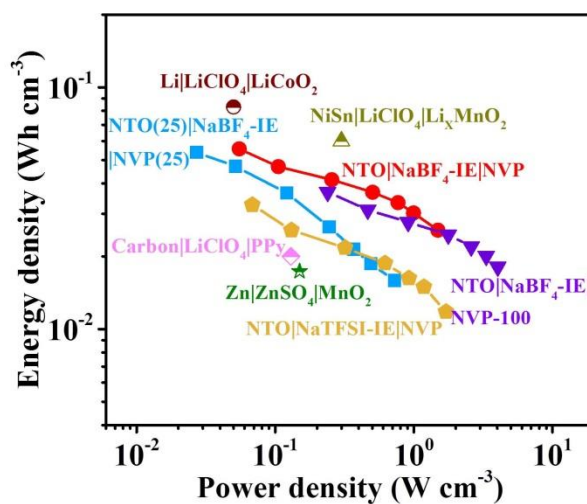


Figure S24. Ragone plot of NTO|NaBF₄-IE|NVP and NTO|NaTFSI-IE|NVP compared with the reported microscale energy storage devices.

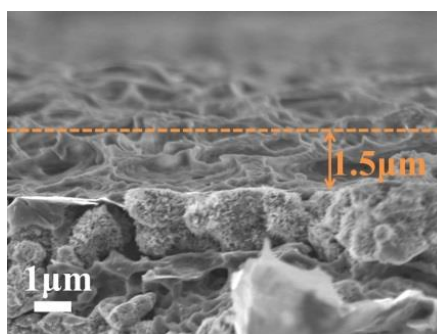


Figure S25. Cross-section SEM image of NTO anode and ionogel electrolyte.

References

- 1 Y. Dong, Z.-S. Wu, S. Zheng, X. Wang, J. Qin, S. Wang, X. Shi and X. Bao, *ACS Nano*, 2017, **11**, 4792-4800.
- 2 Y. Jiang, X. Zhou, D. Li, X. Cheng, F. Liu and Y. Yu, *Adv. Energy Mater.*, 2018, **8**, 1800068.
- 3 Y. L. Zhong and T. M. Swager, *J. Am. Chem. Soc.*, 2012, **134**, 17896-17899.